

 Open access • Posted Content • DOI:10.1101/2021.06.18.448947

Genomic islands targeting *dusA* in *Vibrio* species are distantly related to *Salmonella* Genomic Island 1 and mobilizable by IncC conjugative plasmids — [Source link](#)

Romain Durand, Florence Deschênes, Vincent Burrus

Institutions: Université de Sherbrooke

Published on: 18 Jun 2021 - bioRxiv (Cold Spring Harbor Laboratory)

Topics: Genomic island, Comparative genomics, Plasmid, TRNA modification and Integron

Related papers:

- [Genomic islands targeting *dusA* in *Vibrio* species are distantly related to *Salmonella* Genomic Island 1 and mobilizable by IncC conjugative plasmids.](#)
- [Genomic islands related to *Salmonella* genomic island 1; integrative mobilisable elements in *trmE* mobilised in trans by A/C plasmids](#)
- [A novel family of integrases associated with prophages and genomic islands integrated within the tRNA-dihydrouridine synthase A \(*dusA*\) gene](#)
- [Stability, Entrapment and Variant Formation of *Salmonella* Genomic Island 1](#)
- [Identification and characterization of novel *Salmonella* mobile elements involved in the dissemination of genes linked to virulence and transmission](#)

Share this paper:    

View more about this paper here: <https://typeset.io/papers/genomic-islands-targeting-dusa-in-vibrio-species-are-4ky93lhbxt>

1 **Genomic islands targeting *dusA* in *Vibrio* species are distantly**
2 **related to *Salmonella* Genomic Island 1 and mobilizable by IncC**
3 **conjugative plasmids**

4

5 Romain Durand^{1,#a}, Florence Deschênes¹ and Vincent Burrus^{1*}

6

7 ¹ Département de biologie, Université de Sherbrooke, Sherbrooke, Québec,
8 Canada

9 ^{#a}Current Address: Institut de Biologie Intégrative et des Systèmes, Université
10 Laval, Québec, Canada

11

12 * Corresponding author

13 E-mail: vincent.burrus@usherbrooke.ca

14

15 Short title: *dusA*-specific genomic islands mobilizable by IncC conjugative
16 plasmids

17 **Abstract**

18 *Salmonella* Genomic Island 1 (SGI1) and its variants are significant contributors
19 to the spread of antibiotic resistance among *Gammaproteobacteria*. All known
20 SGI1 variants integrate at the 3' end of *trmE*, a gene coding for a tRNA
21 modification enzyme. SGI1 variants are mobilized specifically by conjugative
22 plasmids of the incompatibility groups A and C (IncA and IncC). Using a
23 comparative genomics approach based on genes conserved among members of
24 the SGI1 group, we identified diverse integrative elements distantly related to
25 SGI1 in several species of *Vibrio*, *Aeromonas*, *Salmonella*, *Pokkaliibacter*, and
26 *Escherichia*. Unlike SGI1, these elements target two alternative chromosomal
27 loci, the 5' end of *dusA* and the 3' end of *yicC*. Although they share many
28 features with SGI1, they lack antibiotic resistance genes and carry alternative
29 integration/excision modules. Functional characterization of IME *VchUSA3*, a
30 *dusA*-specific integrative element, revealed promoters that respond to AcaCD,
31 the master activator of IncC plasmid transfer genes. Quantitative PCR and
32 mating assays confirmed that IME *VchUSA3* excises from the chromosome and is
33 mobilized by an IncC helper plasmid from *Vibrio cholerae* to *Escherichia coli*.
34 IME *VchUSA3* encodes the AcaC homolog SgaC that associates with AcaD to
35 form a hybrid activator complex AcaD/SgaC essential for its excision and
36 mobilization. We identified the *dusA*-specific recombination directionality factor
37 RdfN required for the integrase-mediated excision of *dusA*-specific elements
38 from the chromosome. Like *xis* in SGI1, *rdnN* is under the control of an AcaCD-
39 responsive promoter. Although the integration of IME *VchUSA3* disrupts *dusA*, it

40 provides a new promoter sequence and restores the reading frame of *dusA* for
41 proper expression of the tRNA-dihydrouridine synthase A. Phylogenetic analysis
42 of the conserved proteins encoded by SGI1-like elements targeting *dusA*, *yicC*,
43 and *trmE* gives a fresh perspective on the possible origin of SGI1 and its
44 variants.

45

46 **Author summary**

47 We identified integrative elements distantly related to the *Salmonella* Genomic
48 Island 1 (SGI1), a key vector of antibiotic resistance genes in
49 *Gammaproteobacteria*. SGI1 and its variants reside at the 3' end of *trmE*, share a
50 large, highly conserved core of genes, and carry a complex integron that confers
51 multidrug resistance phenotypes to their hosts. Unlike members of the SGI1
52 group, these novel genomic islands target the 5' end *dusA* or the 3' end of *yicC*,
53 lack multidrug resistance genes, and seem much more diverse. We showed here
54 that, like SGI1, these elements are mobilized by conjugative plasmids of the IncC
55 group. Based on comparative genomics and functional analyses, we propose a
56 hypothetical model of the evolution of SGI1 and its siblings from the progenitor of
57 IncA and IncC conjugative plasmids via an intermediate *dusA*-specific integrative
58 element through gene losses and gain of alternative integration/excision
59 modules.

60 **Introduction**

61 Integrative and mobilizable elements (IMEs) are discrete, mobile chromosomal
62 regions that can excise from the chromosome and borrow the mating apparatus
63 of helper conjugative elements to transfer to a new bacterial host [1,2]. IMEs are
64 usually composed of two main functional modules. The site-specific
65 recombination module contains genes and *cis*-acting sequences that mediate the
66 integration of the IMEs into and their excision from the chromosome. The
67 mobilization module includes the *cis*-acting origin of transfer (*oriT*) and usually
68 encodes mobilization proteins required to initiate the conjugative transfer at *oriT*
69 [1]. In its simplest form, the mobilization module only consists of an *oriT* locus
70 mimicking the *oriT* of the helper element [3–5]. The excision of IMEs is elicited by
71 conjugative plasmids or integrative and conjugative elements (ICEs). These
72 helper elements encode the type IV secretion system (T4SS) that translocates
73 the IME DNA into the recipient cell [1].

74 Several distinct families of IMEs have been described to date. Most encode
75 beneficial traits for their host, such as resistance to antibiotics and heavy metals
76 or bacteriocin synthesis [1,6]. *Salmonella* Genomic Island 1 (SGI1) is certainly
77 one of the most studied IMEs. Though first described 20 years ago, SGI1 and its
78 siblings have only recently gained a lot of attention due to their prevalence and
79 prominent role in the spread of multidrug resistance [7,8]. The canonical 43-kb
80 SGI1 resides at the 3' end of *trmE* (also known as *mnmE* or *thdF*) in *Salmonella*
81 *enterica* serovar Typhimurium DT104 [9]. *trmE* encodes the 5-
82 carboxymethylaminomethyluridine-tRNA synthase GTPase subunit. SGI1

83 variants have been reported in a wide array of *Gammaproteobacteria*, including
84 *Proteus mirabilis* (PGI1), *Acinetobacter baumannii* (AGI1), *Morganella*,
85 *Providencia*, *Enterobacter*, *Escherichia coli*, *Vibrio cholerae* (GI-15), and
86 *Klebsiella pneumoniae* [7,10,11]. Most variants carry a class I integron
87 structurally similar to the In104 integron of SGI1. In104 confers resistance to
88 ampicillin, chloramphenicol/florfenicol, streptomycin/spectinomycin,
89 sulfamethoxazole, and tetracycline [8,12]. SGI1 and its variants are an
90 epidemiological threat exacerbated by their specific mobilization by conjugative
91 plasmids of the incompatibility groups A (IncA) and C (IncC) [13,14]. IncC
92 plasmids contribute to the global circulation of multidrug resistance genes,
93 including NDM metallo- β -lactamase and carbapenemase genes, among a broad
94 range of *Gammaproteobacteria* [15,16]. The transcriptional activator AcaCD
95 encoded by IncC plasmids triggers the excision and mobilization of SGI1 [17,18].

96 SGI1 and most variants share a conserved core set of 28 genes, representing
97 27.4 kb, disrupted by insertion sequences and the class 1 integron inserted at
98 diverse positions (Fig 1, top) [7,9,12]. Thus far, the function of a few conserved
99 genes has been characterized. Together with the *cis*-acting recombination
100 site *attP*, the genes *int* and *xis* form the recombination module of SGI1
101 [13]. *int* encodes the site-specific tyrosine recombinase (integrase) that targets
102 the 3' end of *trmE*. *xis* encodes the recombination directionality factor (RDF or
103 excisionase) that enhances the excision reaction catalyzed by Int. The
104 mobilization module includes the mobilization genes *mpsAB* and the *oriT* located
105 upstream of *mpsA* [19]. *mpsA* encodes an atypical relaxase distantly related to

106 tyrosine recombinases. Unlike most characterized IMEs, SGI1 carries a replicon
107 composed of an iteron-based origin of replication (*oriV*) and the replication
108 initiator gene *rep* [20,21]. SgaCD, a transcriptional activator complex expressed
109 by SGI1 in response to a coresident IncC plasmid, controls *rep* expression
110 [21,22]. The excised replicative form of SGI1 destabilizes the helper plasmid by
111 an unknown process, and is further stabilized by its *sgiAT* addiction module
112 [20,22–24]. Finally, SGI1 encodes three mating pore subunits, TraN_S, TraH_S, and
113 TraG_S, that actively replace their counterparts in the T4SS encoded by the IncC
114 plasmid [25]. The substitution of TraG allows SGI1 to bypass the IncC-encoded
115 entry exclusion mechanism and transfer between cells carrying conjugative
116 plasmids belonging to the same entry exclusion group [26].

117 Given the high similarity between SGI1 variants integrated at *trmE*, we undertook
118 a search for distant SGI1-like IMEs in bacterial genomes using MpsA, TraG_S,
119 SgaC, and TraN_S as baits. Here, we report the existence of distantly related IMEs
120 integrated at the 5' end of *dusA* in several species of *Vibrionaceae* and the 3' end
121 of *yicC* in several species of *Gammaproteobacteria*. We have examined the
122 interactions between an IncC plasmid and IME *VchUSA3*, a *dusA*-specific
123 representative IME from an environmental *V. cholerae* strain. The genetic
124 determinants required for the excision of IME *VchUSA3* and its mobilization by
125 IncC plasmids were characterized. Finally, we took a fresh look at the emergence
126 and evolution of SGI1 and its siblings by conducting phylogenetic analyses and
127 proposed a hypothetical evolutionary pathway of putative IMEs resembling SGI1.

128 **Results**

129 **Novel integrative elements (IEs) distantly related to SGI1 are inserted in** 130 ***dusA* and *yicC* in various *Gammaproteobacteria***

131 To find novel SGI1-like elements, we searched the Refseq database using blastp
132 and the primary sequences of MpsA, TraG_S, SgaC, and TraN_S. Considering the
133 substitution of integration modules can change the integration site [27–29], the
134 integrase Int_{trmE} was excluded from the analysis. We identified 24 distinct
135 integrative elements encoding homologs of the four bait proteins in 36 different
136 bacterial strains (Fig 1, Table 1 and S1 Table). 21 of these IEs are integrated into
137 the 5' end of *dusA* in diverse *Vibrio* species from various origins. The remaining
138 three are located at the 3' end of *yicC* in *E. coli*, *Aeromonas veronii*, *P. mirabilis*,
139 *S. enterica* serovar Kentucky, and *Pokkaliibacter plantistimulans*. The size of the
140 IEs varies from 22.8 kb to 37.1 kb. The conserved genes *mpsA* (together with
141 *mpsB*), *traG*, *traN*, and *sgaC* remain in a syntenic order, though sporadically
142 separated by variable DNA (Fig 1).

143 **Figure 1. Schematic representations of SGI1-related IEs.** The position and
144 orientation of open reading frames (ORFs) are indicated by arrowed boxes.
145 Colors depict the function deduced from functional analyses and BLAST
146 comparisons. Potential AcaCD binding sites are represented by green angled
147 arrows. Each island is flanked by the *attL* and *attR* (vertical grey lines)
148 attachment sites when integrated into the 3' end of *trmE* (light blue), the 5' end of
149 *dusA* (light green), or the 3' end of *yicC* (pink). The annotation of *attL* and *attR*
150 relative to *int* is based on SGI1 (*trmE*) [9], IEAbaD1279779 of *Acinetobacter*

151 *baumannii* D1279779 (*dusA*) [30] and MGI *VflInd1* (*yicC*) [3]. Details regarding
152 ORFs are shown in S1 Dataset.

153 Consistent with the change of integration site, the respective *int* genes of SGI1
154 and the *dusA*- and *yicC*-specific IEs do not share any sequence similarity.
155 Furthermore, unlike SGI1, these novel IEs lack *xis* downstream of *int* (Fig 1).
156 Instead, *yicC*-specific IEs carry two small open reading frames (ORF) upstream
157 of the *attR* site. The putative translation product of the second one shares 35%
158 identity over 65% coverage with the excisionase RdfM of MGI *VflInd1* [31].
159 Although *dusA*-specific IEs lack *xis* and *rdfM*, all carry an ORF predicted to
160 encode a 76-aminoacyl residue protein containing the pyocin activator protein
161 PrtN domain (Pfam PF11112). Based on its size, position, predicted DNA-binding
162 function, conservation, and evidence presented below, we named this ORF *rdfN*.
163 Phylogenetic analysis of Int_{*yicC*} proteins of *yicC*-specific SGI1-like IEs form a
164 cluster distinct from the integrases of IMEs mobilizable by IncC plasmids through
165 a MobI protein (Pfam PF19456), such as MGI *Vmi1*, and IMEs that mimic the *oriT*
166 of SXT/R391 ICEs, such as MGI *VflInd1* [3,17,32] (Fig 2A).

167 **Figure 2. Integrases encoded by the *yicC*- and *dusA*-specific IEs.** Maximum
168 likelihood phylogenetic analyses of Int_{*yicC*} (A) and Int_{*dusA*} (B). The trees are drawn
169 to scale, with branch lengths measured in the number of substitutions per site
170 over 400 and 359 amino acid positions for Int_{*yicC*}, and Int_{*dusA*}, respectively. The
171 helper elements and mechanism of mobilization are indicated for each lineage
172 according to the keys shown in the legend box of panel A. The inset of panel B

173 shows logo sequences of the repeats in *attL* and *attR* attachment sites. The
174 arrows indicate the island termini experimentally determined for IEAbaD1279779
175 by Farrugia *et al.* [30]. (C) Heatmap showing blastp identity percentages of
176 pairwise comparison of Int_{dusA} representative proteins. Proteins accession
177 numbers are provided in S2 Dataset, except for IEAbaD1279779
178 (WP_000534871.1), IEPprPf-5 of *Pseudomonas protegens* Pf-5
179 (WP_011060295.1), and IEs of *Burkholderia gladioli* BSR3 (WP_013697845.1),
180 *Bradyrhizobium* sp. BTAi1 (WP_012043559.1), *Agrobacterium* sp. H13-3
181 (WP_013636109.1), and *Neisseria gonorrhoeae* FA 1090 (EFF39980.1).

182 Phylogenetic analysis of Int_{dusA} proteins confirmed that the integrases of these
183 IEs form a monophyletic group exclusive to the *Vibrionaceae* and distinct from
184 those encoded by other *dusA*-specific IEs found in other taxa, including
185 GIACA Bra1 from *Aeromonas caviae* that is likely mobilizable by IncC plasmids via
186 a MobI protein [32] (Fig 2B). Int_{dusA} proteins of the IEs identified here share at
187 least 75% identity, while identities drop below 60% with the non-*Vibrio* Int_{dusA}
188 proteins (Fig 2C). Sequence logos built using alignments of the *attL* and *attR*
189 chromosomal junctions revealed a 21-bp imperfect repeat at the extremities of
190 each IE (Fig 2B). This repeat is similar to the one reported for *dusA*-specific IEs
191 found in a broader range of species [30].

192 **Three types of *dusA*-integrated SGI1-related elements**

193 Blastn and blastp analyses using SGI1ΔIn104 as the reference confirmed that
194 the identified *dusA*-specific IEs share limited sequence similarities with SGI1
195 (S1A Fig). Besides the genes encoding MpsA, TraG, SgaC, and TraN, all carry

196 the auxiliary mobilization factor gene *mpsB* and the *oriT* sequence (Fig 1).
197 Secondary structure prediction of the aligned *oriT* sequences located upstream
198 of *mpsA* using RNAalifold revealed that despite the sequence divergence, the
199 structure of *oriT* with three stem-loops was strictly conserved (S2B Fig). In
200 contrast, *sgaD* is not strictly conserved and highly divergent from *sgaD* of SGI1
201 when present (Fig 1 and S1A Fig).

202 Comparison using IE *VchUSA2* as the reference suggests that *dusA*-specific IEs
203 cluster into three distinct types as confirmed by the phylogenetic analysis of
204 concatenated *MpsA*-*TraG*-*SgaC*-*TraN* (Fig 3A, S1B and S3 Fig). Type 1 *dusA*-
205 specific IEs such as IME *VchUSA3* are mainly found in *V. cholerae* and lack both
206 *traH* and *sgaD*. Type 2 IEs such as IE *VchUSA2* lack *sgaD* but carry *traH* (Fig 1
207 and 3A). This lineage only includes two *dusA*-specific IEs of *V. cholerae* but also
208 closely related *yicC*-specific IEs such as IE *EcoMOD1* and the *trmE*-specific
209 GI *VchO27-1*. Finally, type 3 IEs such as GI *VchUSA5* are the most distant from
210 the two other types and SGI1 (Fig 3A). Type 3 IEs carry both *traH* and *sgaD* and
211 reside in diverse *Vibrio* species. With the exception of a few outliers encoded by
212 IEs such as IE *VchN2817*, IE *VchN2708* or IE *Pplnd1*, the proteins *MpsA*, *TraG*,
213 *SgaC* and *TraN* encoded by members of the same type typically share more than
214 95% identity (Fig 3B and S3). *MpsA* remains the least divergent protein between
215 the three types, sharing at least 65% identity between type 1 and type 3, and
216 from 64% to 93% with SGI1. In contrast, *TraG* and *TraN* are the most divergent
217 between types, ranging from 46% to 59% for *TraG* and from 46% to 76% for
218 *TraN*.

219 Worthy of note, these three distinct lineages of *dusA*-specific IEs are supported
220 by the phylogeny of the *oriT* sequences (S2A Fig). Again, *oriT* loci of type 3 IEs
221 strongly diverge from those of types 1 and 2, as well as from the *oriT* loci of the
222 highly homogenous SGI1 group.

223 **Figure 3. Conserved genes support three main lineages of *dusA*-specific**
224 **SGI1-like IEs.** (A) Maximum likelihood phylogenetic analysis of concatenated
225 MpsA-TraG-SgaC-TraN. The tree is drawn to scale, with branch lengths
226 measured in the number of substitutions per site over 2,637 amino acid positions.
227 Taxa corresponding to IEs targeting *trmE* and *yicC* are indicated by a light blue
228 circle and a red circle, respectively. All other taxa correspond to *dusA*-specific
229 IEs. Phylogenetic relationships of MpsA, TraG, SgaC and TraN proteins are
230 shown separately in S2 Fig. (B) Heatmaps showing blastp identity percentages of
231 pairwise protein comparisons for representatives of MpsA, TraG, SgaC, and
232 TraN. Proteins accession numbers and clusters are provided in S1 Table and S2
233 Dataset.

234 **Variable features found in the *dusA*- and *yicC*-specific IEs**

235 Most variable genes in the identified IEs encode proteins of unknown function. A
236 search for antibiotic resistance determinants using the Resistance Gene Identifier
237 server failed to reveal any known resistance gene. Several IEs encode putative
238 functions altering host processes and virulence, including the transport of ions
239 and small molecules (*ktrAB*, *trkH*, and *kdpD* for potassium uptake and *rcnAR* for
240 nickel/cobalt efflux in IE *Vch*Hai10, sulfite export in IE *Vch*N2817 and IE *Vch*Swe1),
241 c-di-GMP degradation (IE *Vch*Ban1), and fimbriae (IE *Vch*Ban1) (S1 Dataset).

242 None of the reported IEs carries the same replication module (*S004-rep-oriV*) as
243 canonical SGI1. Instead, five *dusA*-specific IEs belonging to the type 3 lineage
244 (IE *VchUSA5*, IE *VchBra2*, IE *VpaChn1*, IE *VpaChn2*, and IE *VpaBan1a*) encode a
245 putative replication initiator protein with the IncFII_repA domain (Pfam PF02387)
246 (Fig 1, S1 Dataset). IE *VvuUSA1* encodes a putative helicase with an UvrD_C_2
247 domain (Pfam PF13538), whereas IE *VchHai10*, IE *VchUSA2* and IE *VchSwe1*
248 encode a putative ATP-dependent helicase (PcrA) and a putative ATP-
249 dependent endonuclease (YbjD). In addition, IE *VchN2786*, IE *SenUSA1* and
250 IE *EcoMOD1* encode a predicted DEAD/DEAH box helicase (Pfam PF00270 and
251 PF00271). The three *yicC*-specific IEs encode a homolog of TrfA (Pfam
252 PF07042), the replication initiator protein of broad-host-range IncP plasmids [33].
253 No replicative functions could be ascribed with confidence to any gene carried by
254 the other *dusA*-specific IEs. Several IEs also encode toxin-antitoxin systems,
255 such as *sgiAT* and *higAB*, which likely enhance their stability (Fig 1). In the type 3
256 IEs IE *VchBra2*, IE *VchN2708*, IE *VpaChn1* and IE *VpaBan1a*, *sgiAT* is associated
257 with a gene coding for a putative abortive infection bacteriophage resistance
258 factor (*Abi_2*, Pfam PF07751). Likewise, IE *VvuUSA1* carries a gene coding for a
259 different putative abortive infection bacteriophage resistance factor (*AbiEii* toxin,
260 Pfam PF13304).

261 Finally, IE *VpaBan1a* is integrated at *dusA* adjacent to a distinct IE, IE *VpaBan1b*,
262 in a tandem fashion. GI *VpaBan1b* codes for two predicted integrases sharing
263 44% and 27% identity with Int_{*dusA*} of IE *VpaBan1a*. GI *VpaBan1b* encodes a

264 putative type I restriction-modification system, a MobA-like relaxase (MOB_{P1}), the
265 mobilization auxiliary factor MobC, and an RdfN homolog (Fig 1).

266 **Non-canonical SGI1-like IEs carry AcaCD-responsive genes**

267 Considering the divergence of the 24 new IEs from prototypical SGI1, we
268 wondered whether an IncC plasmid could mobilize them like SGI1. The hallmark
269 of IncC-dependent mobilization is the presence of AcaCD-responsive promoters
270 in IncC-mobilizable IEs. Hence, we searched for putative AcaCD-binding sites in
271 the sequences of *trmE*-specific IEs (prototypical SGI1 was used as the positive
272 control) and the *yicC*- and *dusA*-specific IEs. In these IEs, an AcaCD-binding
273 motif was predicted upstream of *traN*, *traHG* (or *traG*), *S018*, and *xis* (or *rdfM* or
274 *rdfN*) (Fig 1 and S4 Fig). Moreover, an AcaCD-binding motif was also predicted
275 upstream of *trfA* in the *yicC*-specific IEs.

276 We cloned the promoter sequences of *int*, *traN*, *traG*, *S018*, and *rdfN* of
277 IME *VchUSA3* upstream of a promoterless *lacZ* reporter gene and monitored the
278 β -galactosidase activity with or without AcaCD. The promoter P_{int} was active
279 regardless of the presence of AcaCD (Fig 4A). In contrast, the four other
280 promoters exhibited weak activity in the absence of AcaCD. Upon induction of
281 *acaDC* expression, P_{traN} and P_{S018} remained unresponsive, while the activities of
282 P_{traG} and P_{rdfN} increased 40 and 400 times, respectively (Fig 4B). The inertia of
283 P_{traN} and P_{S018} toward AcaCD could result from single nucleotide substitutions in
284 the AcaCD binding site previously shown to be essential for recruiting the
285 activator [22]: CC~~S~~AAAWW instead of CCSCAAWW in P_{traN} and CCCCAAAA instead of
286 CCC~~A~~AAAA in P_{S018} (S4 Fig).

287 **Figure 4. β -galactosidase activities of the promoters P_{int} , P_{traN} , P_{traG} , P_{S018}**
288 **and P_{rdfN} of IME *VchUSA3* transcriptionally fused to *lacZ*.** (A) Colonies were
289 grown on LB agar with or without arabinose to induce *acaDC* expression from
290 pBAD-*acaDC*. (B) Induction levels of the same promoters in response to AcaCD.
291 β -galactosidase assays were carried out using the strains of panel A. Ratios
292 between the enzymatic activities in Miller units for the arabinose-induced versus
293 non-induced strains containing pBAD-*acaDC* are shown. The bars represent the
294 mean and standard error of the mean of three independent experiments.

295 Hence, despite their divergence and different integration sites, these IEs share
296 with SGI1 a common activation mechanism elicited by the presence of an IncC
297 plasmid.

298 **IncC plasmids induce the excision and mobilization of IME *VchUSA3***

299 Next, we tested whether a coresident IncC plasmid could trigger the excision of
300 IME *VchUSA3* from *dusA* in its original host, *V. cholerae* OY6PG08. The
301 derepressed IncC plasmid pVCR94^{Kn} Δ *acr2* [34] was introduced into OY6PG08
302 by conjugation from *E. coli* KH40. The Δ *acr2* mutation improves the efficiency of
303 interspecific transfer of the plasmid [35]. OY6PG08 Kn^R transconjugants were
304 tested by PCR to amplify the *attL* and *attR* chromosomal junctions, as well as the
305 *attB* and *attP* sites resulting from the excision of IME *VchUSA3* (S5A Fig).
306 IME *VchUSA3* was rarely retained in the transconjugants compared to the control
307 IncC-free OY6PG08 clones, suggesting it was unstable and rapidly lost in IncC⁺
308 cells (S5B and S5C Figs).

309 To test the interspecific mobilization of IME *VchUSA3* from *V. cholerae*
310 OY6PG08, we inserted a selection marker upstream of *traG* and used pVCR94^{Kn}
311 Δ *acr2* as the helper plasmid. IME *VchUSA3*^{Cm} transferred to *E. coli* CAG18439 at
312 a frequency of 7.01×10^{-5} transconjugant/donor CFUs. Amplification of *attL* and
313 *attR* using *E. coli*-specific primers confirmed that IME *VchUSA3* integrates at
314 *dusA* in *E. coli* (S5D Fig).

315 **Excision of *dusA*-specific IEs depends on *rdfN***

316 To further characterize the biology of IME *VchUSA3*, we measured its excision
317 rate and copy number by qPCR, with and without coresident pVCR94^{Sp}. We also
318 monitored its intraspecific transfer (*E. coli* to *E. coli*) in the same context.
319 Spontaneous excision of the island rarely occurred (<0.001% of the cells) (Fig
320 5A). In contrast, in the presence of the helper plasmid, the free *attB* site was
321 detected in more than 67% of the cells confirming that the IncC plasmid elicits
322 the excision of IME *VchUSA3*^{Kn}. Likewise, the presence of the plasmid resulted in
323 a ~3-fold increase of the copy number of IME *VchUSA3*^{Kn} (Fig 5B), suggesting
324 that the excised form of the island undergoes replication. The frequency of
325 transfer of IME *VchUSA3*^{Kn} was comparable to that of the helper plasmid
326 ($\sim 3.5 \times 10^{-2}$ transconjugants/donor), while the frequency of cotransfer was more
327 than two logs lower (Fig 5C).

328 **Figure 5. Effect of *acaDC* and *rdfN* on the IncC-dependent excision and**
329 **mobilization of IME *VchUSA3*.** (A) IME *VchUSA3*^{Kn} excision rate corresponds to
330 the *attB*/chromosome ratio. (B) IME *VchUSA3*^{Kn} copy number corresponds to the
331 *higA*/chromosome ratio. For panels A and B, all ratios were normalized using the

332 control set to 1 and displayed in white. (C) Impact of *acaC*, *acaDC*, *sgaC* and
333 *rdfN* deletions on the mobilization of IME *VchUSA3*. Conjugation assays were
334 performed with CAG18439 (Tc) containing the specified elements as donor
335 strains and VB112 (Rf) as the recipient strain. The bars represent the mean and
336 standard error of the mean obtained from a biological triplicate. □ indicates that
337 the excision rate or transfer frequency was below the detection limit. Statistical
338 analyses were performed (on the logarithm of the values for panels A and C)
339 using a one-way ANOVA with Dunnett's multiple comparison test. For panels A
340 and B, statistical significance indicates comparisons to the normalization control.
341 Statistical significance is indicated as follows: ****, $P < 0.0001$; ***, $P < 0.001$; **, $P < 0.01$;
342 *, $P < 0.05$; ns, not significant. (D) Schematic representation of mini-IE
343 inserted at the 5' end of *dusA*. (E) RdfN acts as a recombination directionality
344 factor. Detection of *attB*, *attP*, *attL* and *attR* sites by PCR in colonies of *E. coli*
345 EC100 *dusA::mini-IE* in the presence or absence of *rdfN*. L, 1Kb Plus DNA
346 ladder (Transgen Biotech).

347 Thus far, the factors required to catalyze the excision of *dusA*-specific IEs have
348 not been examined [30]. Whereas all *dusA*-specific IEs lack *xis* downstream of
349 *int*, they carry a small ORF, here named *rdfN*, coding for a putative PrtN homolog
350 (Fig 1) [30]. The deletion of *rdfN* abolished the excision and replication of
351 IME *VchUSA3*^{Kn}. Complementation by ectopic expression of *rdfN* from the
352 arabinose-inducible promoter P_{BAD} restored the wild-type excision level but not
353 the replication (Fig 5A and 5B). Likewise, deletion of *rdfN* abolished the

354 mobilization of IME *VchUSA3*^{Kn} but had no impact on the transfer of the helper
355 plasmid (Fig 5C), confirming the specific role of *rdfN* in the IE's mobility.
356 To confirm that *rdfN* encodes the sole and only RDF of IME *VchUSA3*, we
357 constructed mini-IE, a minimal version of IME *VchUSA3* that only contains *int* and
358 a spectinomycin-resistance marker. mini-IE is flanked by *attL* and *attR* and is
359 integrated at *dusA* in *E. coli* EC100 (Fig 5D). Using mini-IE, *attB* and *attP* were
360 detected only upon ectopic expression of *rdfN* from pBAD-*rdfN*, confirming that
361 no other IME *VchUSA3*-encoded protein besides Int and RdfN is required for the
362 excision of the element (Fig 5E). *rdfN* is the essential RDF gene that favors the
363 excision of IME *VchUSA3* and, most likely, all *dusA*-specific IEs.

364 **A SgaC/AcaD hybrid complex activates the excision and mobilization of** 365 **IME *VchUSA3***

366 Next, we investigated the role of the transcriptional activator genes *acaC* and
367 *sgaC* in the mobilization of IME *VchUSA3*. Deletion of *acaDC* abolished the
368 excision and replication of IME *VchUSA3*^{Kn}, confirming that its excision relies on
369 *rdfN*, whose expression is activated by AcaCD (Figs 4, 5A and 5B). The mutation
370 also confirmed that SgaC provided by IME *VchUSA3*^{Kn} is insufficient by itself to
371 elicit *rdfN* expression. The excision rate remained extremely low in cells that lack
372 the helper plasmid or cells that carry pVCR94^{Sp} Δ *acaDC*. However,
373 IME *VchUSA3*^{Kn} allowed the low-frequency transfer of pVCR94^{Sp} Δ *acaDC* [17]
374 (Fig 5C). Hence SgaC alone can activate to some degree the expression of the
375 transfer genes of the helper plasmid. In contrast, deletion of *acaC* had no
376 significant impact on the excision, replication, and mobilization of

377 IME *VchUSA3*^{Kn}, or on the transfer of the helper plasmid (Figs 5A, 5B and 5C).
378 The primary sequences of *AcaC* and *SgaC* from IME *VchUSA3* share 85%
379 identity over 94% coverage, whereas *AcaC* and *SgaC* from SGI1 share only 75%
380 identity over 92% coverage. Hence *AcaD* produced by the plasmid and *SgaC*
381 produced by the IME likely generate a functional chimeric transcriptional complex
382 that acts as a potent activator of *rdfN* and the transfer genes.

383 The transfer of IME *VchUSA3*^{Kn} Δ *sgaC* decreased nearly 3 logs compared to the
384 wild-type IE, despite the presence of *acaDC* on the helper plasmid (Fig 5C).
385 Moreover, deletion of both *acaC* and *sgaC* nearly abolished all transfer. Ectopic
386 expression of *sgaC* alone from pBAD-*sgaC* complemented these deletions to
387 wild-type levels (Fig 5C). These observations confirm that *sgaC*, not *acaC*,
388 combined with *acaD* produces a hybrid activator complex that is essential for the
389 excision and mobilization of the element.

390 **IME *VchUSA3* provides a new promoter and N-terminus for *dusA*** 391 **expression**

392 Since *dusA*-specific IEs insert within the 5' end of *dusA*, we wondered whether
393 the gene remains expressed after the integration event. Sequence analysis of the
394 *attR* junction of *E. coli* K12 transconjugants revealed that IME *VchUSA3* provides
395 a new 5' coding sequence that diverges significantly from the native *E. coli* *dusA*
396 gene (Fig 6A). This alteration of the 5' end of *dusA* results in a novel N-terminus
397 of identical length sharing 61% identity over the 35 initial amino acid residues
398 with native *DusA*. To test the expression of *dusA*, we constructed a translational
399 *lacZ* fusion to its fortieth codon downstream of the *attR* junction in *E. coli*

400 CAG18439 and BW25113 (Fig 6B). β -galactosidase assays revealed that *dusA*
401 remains expressed after integration in both strains, confirming that IME *VchUSA3*
402 provides a new promoter (Fig 6C). However, we observed a statistically
403 significant reduction of *dusA* expression resulting from the integration of the IE in
404 both strains, suggesting that the transcription or translation signals brought by
405 the IE are weaker than the original ones upstream of *E. coli dusA*.

406 **Figure 6. IME *VchUSA3* drives the expression of *dusA*.** (A) Comparison of the
407 coding sequences of the 5' end of *dusA* in *E. coli* K12 MG1655 before (*attB* site)
408 and after (*attL* junction) the integration of IME *VchUSA3*. The core sequence of
409 the *attB* and *attL* recombination sites is indicated with red shading. The ATG start
410 codon of *dusA* is shown in bold. The sequence shown in blue is internal to
411 IME *VchUSA3*. Amino acid residues shown in red differ from the native N-
412 terminus of *DusA*. This sequence was obtained by sequencing the *attL* junction
413 of an *E. coli* CAG18439 *dusA::IME VchUSA3^{Kn}* transconjugant colony. (B)
414 Schematic representation of the *dusA'*-*lacZ* translational fusion for the detection
415 of *dusA* expression. (C) β -galactosidase activity of the *dusA'*-*lacZ* fusion before
416 (-) and after (+) insertion of IME *VchUSA3^{Kn}* in *E. coli* CAG18439 (FD034) and
417 BW25113 (FD036). The bars represent the mean and standard error of the mean
418 of three independent experiments. Statistical analyses were performed using an
419 unpaired *t* test to compare the expression before and after integration of
420 IME *VchUSA3^{Kn}* for each strain. Statistical significance is indicated as follows: **,
421 $P < 0.01$; *, $P < 0.05$.

422 **Discussion**

423 SGI1-like elements integrated at the 3' end of *trmE* are widespread in a broad
424 range of *Enterobacteriaceae* and sporadically found in a few *Vibrio* species [7].
425 The integrase of SGI1 and its variants occasionally targets the intergenic region
426 between *sodB* and *purR* genes, a secondary attachment site [36]. Here, we
427 report the identification of distant SGI1-like elements that specifically target the 5'
428 end of *dusA* in multiple *Vibrio* species and the 3' end of *yicC* in
429 *Enterobacteriaceae* and *Balneatricaceae*. Farrugia *et al.* [30] already described
430 IEs integrated at the 5' end of *dusA*, mostly prophages or phage remnants found
431 exclusively in *Alpha-*, *Beta-* and *Gammaproteobacteria*. These authors identified
432 IE *VchBan1a* and IE *VchBra2* in *V. cholerae*, and several other IEs predicted to
433 encode conjugative functions in *Bradyrhizobium*, *Caulobacter*, *Mesorhizobium*,
434 *Paracoccus*, *Pseudomonas*, and *Rhodocyclops* [30]. Our group recently
435 reported a *dusA*-specific IE in *Aeromonas caviae* 8LM potentially mobilizable by
436 IncC plasmids [32]. *GIAca8LM* lacks *tra* genes but encodes a mobilization protein
437 (MobI) under the control of an AcaCD-responsive promoter. Together, these
438 reports confirm that *dusA* is an insertion hotspot for distinct families of mobile
439 elements across at least three *Proteobacteria* phyla.

440 Thus far, only the *dusA*-specific IEs in *A. baumannii* D1279779 and *P. protegens*
441 Pf-5 were shown to excise from the chromosome, albeit at a low level [30].
442 Neither IE has been tested for intercellular mobility. Here, we characterized
443 IME *VchUSA3*, a representative member of a subgroup of *dusA*-specific IEs
444 circulating in *Vibrio* species and distantly related to SGI1. We demonstrated that

445 IME *VchUSA3* is mobilizable by IncC conjugative plasmids to *E. coli*. In the
446 presence of an IncC plasmid, this IME excises in practically all cells of the
447 population and becomes highly unstable (Figs 5B and 6A). We showed that its
448 excision was under the control of AcaCD provided by the IncC plasmid and
449 required *rdfN*, a gene whose expression is driven by an AcaCD-responsive
450 promoter (Fig 4). *rdfN* encodes a novel RDF distantly related to the pyocin
451 activator protein PrtN of *Pseudomonas*. *rdfN* seems to be ubiquitous, yet highly
452 divergent, in *dusA*-specific IEs reported by Farrugia *et al.* [30]. For instance,
453 RdfN (PrtN) encoded by the IE of *P. protegens* Pf-5 shares only 29% identity with
454 RdfN of IME *VchUSA3*, and their promoters are unrelated. Hence, the expression
455 of *rdfN* homologs encoded by different families of *dusA*-specific IEs is likely
456 controlled by different factors. Only the IEs that have evolved AcaCD-responsive
457 promoters for their RDF gene are expected to be mobilizable by IncC or related
458 plasmids.

459 Excision and mobilization of IME *VchUSA3* occurred in the presence of a Δ *acaC*
460 but not a Δ *acaDC* mutant of the helper plasmid (Fig 5), confirming that *sgaC* of
461 the IME produces a functional activator subunit that can interact with AcaD
462 provided by the plasmid. Furthermore, we showed here that, unlike *acaC*, *sgaC*
463 plays a central role in the biology of IME *VchUSA3* as the absence of *acaC* had
464 no effect on the excision or transfer of the IME, while the absence of *sgaC* in
465 spite of the presence of *acaC*, compromised its mobilization (Figs 5A, 5B and
466 5C). We recently showed that AcaD most likely stabilizes the binding of AcaC to
467 the DNA [22]. Therefore, AcaD and SgaC from IME *VchUSA3* likely interact to

468 form a chimerical activator complex. This interaction could compensate for the
469 loss of *sgaD* in *yicC*- and type 1 and 2 *dusA*-specific IEs (Fig 1). The primary
470 sequences of AcaC and SgaC of IME *VchUSA3* (type 1) share 85% identity. In
471 contrast, AcaC only shares 75% identity with SgaC of SGI1 and 64% identity with
472 SgaC of GI *VchUSA5* (type 3), suggesting that retention of *sgaD* allowed faster
473 divergence of SgaC from AcaC. Retention of *sgaC* in the IEs could result from its
474 essential role as the elicitor of excision and replication reported for SGI1. Indeed,
475 although AcaCD binds to the promoters P_{xis} and P_{rep} of SGI1, it fails to initiate
476 transcription at these two promoters, unlike SgaCD [22]. Nonetheless, P_{xis} and
477 P_{rep} are not conserved in the IEs described here. *S004-rep* is missing, whereas
478 *rdfN* or *rdfM* replaced *xis* with novel AcaCD-responsive promoters (Fig 4 and S3
479 Fig). This observation raises intriguing questions regarding the recruitment of
480 functional gene cassettes and their assimilation in a regulatory pathway. How did
481 *xis*, *rdfN*, and *rdfM* acquire their AcaCD-responsive promoters? Is it by
482 convergent evolution? What are the signals driving *rdfN* expression and IE
483 excision in *dusA*-specific IEs resembling prophages?

484 Approximately 3 copies per cell of IME *VchUSA3* were detected in the presence
485 of the helper IncC plasmid (Fig 5B), lower than the copy number reported for
486 SGI1 (~8 copies/cell) [20,22]. IME *VchUSA3* lacks SGI1's replication module
487 (*S004-rep-oriV*); however, one of the multiple genes of unknown function could
488 encode an unidentified replication initiator protein. Notably, GI *VchO27-1* encodes
489 a putative replication protein with an N-terminal replicase domain (PF03090) and
490 a C-terminal primase domain (PriCT-1, PF08708) [20]. Multiple IEs also carry

491 putative replicons based on *repA* and *trfA* (Fig 1), suggesting that independent
492 replication is crucial in their lifecycle, perhaps to improve their stability in the
493 presence of a helper plasmid [20–24].

494 Farrugia *et al.* [30] hypothesized that *dusA*-specific IEs could restore the
495 functioning of *DusA*. We demonstrated here that IME *VchUSA3* provides a new
496 promoter allowing expression of *dusA*, though at a lower level than in IME-free
497 cells, and restores the open reading frame with an altered N-terminus (Fig 6).
498 Similarly, the ICE SXT that targets the 5' end of the peptide chain release factor
499 3 (RF3) gene *prfC* provides a new promoter and N-terminus in both *V. cholerae*,
500 its original host, and *E. coli* [37]. In both cases, the consequences of the
501 alteration of the N-terminus on the activity of the protein remain unknown.

502 The relative positions of *int* and *rdfN/rdfM* across the *attP* site suggest that, to
503 remain functional, the recombination modules must be acquired or exchanged
504 when the IEs are in their excised circular form. The promiscuity of different
505 families of IEs targeting *yicC*, *dusA*, and *trmE* and mobilizable by IncC plasmids
506 could act as the catalyst for these recombination events. During entry into a new
507 host cell by conjugation, IncC plasmids elicit the excision of such IEs and
508 promote homologous recombination between short repeated sequences in
509 response to double-stranded break induced by host defense systems (CRISPR-
510 Cas3) [34]. Hence the diversification of IncC plasmid-mobilizable IEs could be a
511 side effect of the DNA repair mechanism used by these plasmids.

512 Unlike SGI1 and its siblings, all *dusA*-specific SGI1-like IEs reported here lack
513 antibiotic resistance genes. Furthermore, SGI1 variants are prevalent in several
514 pathogenic species and relatively well-conserved, whereas their *dusA*-specific
515 relatives are scarce and highly divergent. These observations suggest that
516 despite the considerable functional resemblances between *trmE*- and *dusA*-
517 specific SGI1-like IEs, the epidemiological success of the SGI1 lineage has
518 directly stemmed from the acquisition of class I integrons conferring multidrug
519 resistance by forerunner elements such as SGI0 [38]. Based on the phylogenetic
520 relationships between the core proteins MpsA, TraG, SgaC and TraN, *oriT* loci,
521 and integrase proteins (Figs 2 and 3, and S2A and S3 Figs), we propose a
522 hypothetical evolutionary pathway leading to the emergence of the different types
523 of IEs described here (Fig 7). The diversity of *dusA*-specific IEs and relative
524 homogeneity of the SGI1 group suggest that the latter originated from the
525 progenitor of IncA and IncC plasmids via a *dusA*-specific IE intermediate.

526 **Figure 7. Proposed hypothetical evolutionary pathway of SGI1-like IEs.** The
527 sequence of events was inferred from the phylogenetic trees presented in this
528 study, site of integration and conservation of *traH* and *sgaD* in the IEs. The
529 proposed pathway ignores the gene cargo and presumes that the IE lineages
530 evolved from the progenitor of IncA and IncC plasmids. The *dusA*-specific
531 recombination module was chosen as the progenitor to minimize gain/loss and
532 recombination events. Green and red arrows indicate gene gains and losses,
533 respectively. The orange dashed line indicates a probable recombination event
534 from which stemmed GIVchO27-1.

535 **Materials and Methods**

536 **Bacterial strains and media**

537 Bacterial strains and plasmids used in this study are described in Table 2. Strains
538 were routinely grown in lysogeny broth at 37°C in an orbital shaker/incubator and
539 were preserved at -75°C in LB broth containing 20% (vol/vol) glycerol. Antibiotics
540 were used at the following concentrations: ampicillin (Ap), 100 µg/ml;
541 chloramphenicol (Cm), 20 µg/ml; erythromycin (Em), 200 µg/ml; kanamycin (Kn),
542 10 µg/ml for single-copy integrants of pOP/*acZ*-derived constructs, 50 µg/ml
543 otherwise; nalidixic acid (Nx), 40 µg/ml; rifampicin (Rf), 50 µg/ml; spectinomycin
544 (Sp), 50 µg/ml; tetracycline (Tc), 12 µg/ml. Diaminopimelate (DAP) was
545 supplemented to a final concentration of 0.3 mM when necessary.

546 **Mating assays**

547 Conjugation assays were performed as previously described [25]. However,
548 mixtures of donor and recipient cells were incubated on LB agar plates at 37°C
549 for 4 hours. Donors and recipients were selected according to their sole
550 chromosomal markers. When required, mating experiments were performed
551 using LB agar plates supplemented with 0.02% arabinose to induce expression
552 of pBAD30-derived complementation vectors. Frequencies of transconjugant
553 formation were calculated as ratios of transconjugant per donor CFUs from three
554 independent mating experiments.

555 **Molecular biology**

556 Plasmid DNA was prepared using the QIAprep Spin Miniprep Kit (Qiagen),
557 according to manufacturer's instructions. Restriction enzymes used in this study

558 were purchased from New England Biolabs. Q5 DNA polymerase (New England
559 Biolabs) and EasyTaq DNA Polymerase (Civic Bioscience) were used for
560 amplifying cloning inserts and verification, respectively. PCR products were
561 purified using the QIAquick PCR Purification Kit (Qiagen), according to
562 manufacturer's instructions. *E. coli* was transformed by electroporation as
563 described by Dower *et al.* [39] in a Bio-Rad GenePulser Xcell apparatus set at 25
564 μF , 200 Ω and 1.8 kV using 1-mm gap electroporation cuvettes. Sanger
565 sequencing reactions were performed by the Plateforme de Séquençage et de
566 Génotypage du Centre de Recherche du CHUL (Québec, QC, Canada).

567 **Plasmids and strains constructions**

568 Plasmids and oligonucleotides used in this study are listed in Table 2 and S2
569 Table, respectively. IME *VchUSA3*^{Cm} was constructed by inserting the *pir*-
570 dependent replication RP4-mobilizable plasmid pSW23T [40] at locus
571 CGT85_RS05425 of *V. cholerae* OYP6G08 (Genbank NZ_NMSY01000009) by
572 homologous recombination. Briefly, CGT85_RS05425 was amplified using primer
573 pair dusAigEcoRIF/dusAigEcoRIR. The amplicon was digested with EcoRI and
574 cloned into EcoRI-digested pSW23T using T4 DNA ligase. The resulting plasmid
575 was confirmed by restriction profiling and DNA sequencing, then introduced into
576 the DAP-auxotrophic *E. coli* β 2163 [40] by transformation. This strain was used
577 as a donor in a mating assay to transfer the plasmid into *V. cholerae* OYP6G08,
578 generating IME *VchUSA3*^{Cm}. Single-copy integration of the pSW23T derivative
579 was confirmed by PCR and antibiotic resistance profiling.

580 IME *VchUSA3*^{Kn} was constructed from IME *VchUSA3*^{Cm}. Briefly, pVCR94^{Kn} Δ *acr2*
581 was transferred from the DAP-auxotrophic *E. coli* KH40 into OYP6G08 bearing
582 IME *VchUSA3*^{Cm}. After selection on LB agar medium supplemented with
583 chloramphenicol and kanamycin, Cm^R Kn^R *V. cholerae* OYP6G08
584 transconjugants were confirmed by growth on thiosulfate-citrate-bile salts-
585 sucrose (TCBS) agar medium (Difco). In *V. cholerae*, the integration and excision
586 of the IME were confirmed by amplification of the *attL*, *attR*, *attB*, and *attP* sites
587 with primer pairs oRD4/ORD6, oRD1/oRD3, oRD1/oRD6, and oRD4/oRD3,
588 respectively. IME *VchUSA3*^{Cm} was then mobilized from OYP6G08 to *E. coli*
589 CAG18439. In *E. coli*, the integration and excision of the IME were confirmed by
590 amplification of the *attL*, *attR*, *attB* and *attP* sites with primer pairs oRD4/ORD5,
591 oRD2/oRD3, oRD2/oRD5 and oRD4/oRD3, respectively. IME *VchUSA3*^{Kn} was
592 constructed by replacing pSW23T with a single kanamycin resistance marker
593 using the one-step chromosomal gene inactivation technique with primer pair
594 *dusAscarNoFRTf/dusAscarNoFRT*r and pKD13 as the template. The deletions
595 Δ *sgaC* and Δ *prtN* in IME *VchUSA3*^{Kn} were obtained using the primer pairs
596 oFD26r/oFD26f and *DelprtNr/DelprtNf*, and pKD3 and pVI36 as the templates,
597 respectively. The Δ *dapA* deletion mutant of *E. coli* MG1655 was constructed
598 using primer pair *FwDeltaDapA-MG1655/ RvDeltaDapA-MG1655* and pKD3 as
599 the template. The Δ *lacZ* mutation was introduced in *E. coli* CAG18439 using
600 primer pair *lacZW-B/lacZW-F* and plasmid pKD4 as the template. The *dusA*'-
601 '*lacZ* fusion was introduced in *E. coli* BW25113 and CAG18439 using primer pair
602 oDF15/oDF16 and pVI42B as the template. The fortieth codon of *dusA* was fused

603 to the eighth codon of *lacZ* downstream of the *attB* site. The λ Red recombination
604 system was expressed using either pSIM6, pSIM9 or pKD46 [41,42]. When
605 appropriate, resistance cassettes were excised from the resulting constructions
606 using the Flp-encoding plasmid pCP20 [43]. All deletions were validated by
607 antibiotic profiling and PCR.

608 Fragments encompassing promoter regions upstream of *int*, *traN*, *traG*, *s018* and
609 *rdfN* were amplified using primer pairs oFD6.f/oFD6.r, oFD1.f/oFD1.r,
610 oFD3.f/oFD3.r, oFD5.f/oFD5.r and oFD4.f/oFD4.r, respectively, and genomic
611 DNA from *E. coli* CAG18439 *dusA::IME VchUSA3^{Kn}* as the template. The
612 amplicons were digested with PstI/XhoI and cloned into PstI/XhoI-digested
613 pOP/*lacZ* [17]. The resulting constructs were single-copy integrated into the *attB_λ*
614 chromosomal site of *E. coli* BW25113 using pINT-ts [44]. To construct the
615 expression vectors pBAD-*rdfN* and pBAD-*sgaC*, PCR fragments containing *rdfN*
616 or *sgaC* were amplified from genomic DNA of *E. coli* CAG18439 bearing
617 IME *VchUSA3* as the template and primer pairs prtNEcoRII/prtNHindIIIrev and
618 oFD38r/oFD44f, respectively. The PCR fragments were digested by either EcoRI
619 or SacI, and HindIII and cloned into pBAD30 cut with the same enzymes.

620 mini-IE was constructed as follows. The 1,591-bp fragment of excised circular
621 IME *VchUSA3^{Kn}* that contains *attP-int* was amplified using primer pair
622 oVB12/oVB10 and genomic DNA from *E. coli* CAG18439 *dusA::IME VchUSA3^{Kn}*
623 as the template. The 1,421-bp fragment of pVI36 that contains *aadA7* was
624 amplified using primer pair oVB11/oVB13. Both fragments were joined using the
625 PCR-based overlap extension method [45]. After the final PCR amplification

626 using oVB12/oVB13, the amplicon was purified, digested with *SacI*, and ligated.
627 The ligation mixture was then transformed into *E. coli* EC100. Transformant
628 colonies were selected on LB agar supplemented with spectinomycin. The
629 constitutive expression of *int* and the absence of replicon prompted the
630 spontaneous integration of mini-IE at the 5' end of *dusA* in EC100.

631 All final constructs were verified by PCR and DNA sequencing by the Plateforme
632 de Séquençage et de Génotypage du Centre de Recherche du CHUL (Québec,
633 QC, Canada).

634 **qPCR assays**

635 qPCR assays for quantification of excision and copy number of IME *VchUSA3*^{Kn}
636 were carried out as described previously [22] with the following modification.
637 *attB_{dusA}* (241 bp) and *higA* (229 bp) of IME *VchUSA3*^{Kn} were quantified using
638 primer pairs *attB_{dusA}qPCRfwd/ attB_{dusA}qPCRrev* and *higAqPCRfwd/*
639 *higAqPCRrev*, respectively (S2 Table). The excision rate and copy number of
640 IME *VchUSA3*^{Kn} were calculated as the ratio of free *attB_{dusA}* site per chromosome
641 and as the ratio of *higA* per chromosome, respectively. The data were analyzed
642 and normalized using all three chromosomal genes *dnaB*, *hicB* and *trmE* as
643 references and the qBase framework as described previously [22,46].

644 **β-galactosidase assays**

645 The assays were carried out on LB agar plates supplemented with 5-bromo-4-
646 chloro-3-indolyl-β-D-galactopyranoside (X-gal) or in LB broth using *o*-nitrophenyl-
647 β-D-galactopyranoside (ONPG) as the substrate as described previously [32].

648 *acaDC* expression from pBAD-*acaDC* was induced by adding 0.2% arabinose to
649 a refreshed culture grown to an OD₆₀₀ of 0.2, followed by a 2-h incubation at
650 37°C with shaking prior to cell sampling.

651 **Comparative analyses**

652 Sequences were obtained using blastp against the Genbank Refseq database
653 with the primary sequences of key proteins MpsA, TraG_S, SgaC, TraN_S of SGI1
654 (Genbank AAK02039.1, AAK02037.1, AAK02036.1, AAK02035.1, respectively),
655 and Int_{*dusA*} of IE *VchBra2* (Genbank EEO15317.1) and Int_{*yicC*} of IE *EcoMOD1*
656 (Genbank WP_069140142.1). Hits were exported, then sorted by accession
657 number to identify gene clusters that likely belong to complete IEs. Sequences of
658 IEs were manually extracted and the extremities were identified by searching for
659 the direct repeats contained in *attL* and *attR* sites. When an IE sequence
660 spanned across two contigs (e.g., IE *VchHai10* and IE *PplInd1*), the sequence was
661 manually assembled. IE sequences were clustered using cd-hit-est with a 0.95
662 nucleotide sequence identity cut-off [47]. Some of the annotated sequences were
663 manually curated to correct missing small open reading frames such as *mpsB*,
664 and inconsistent start codons. Pairwise comparisons of Int, MpsA, TraG, SgaC
665 and TraN proteins were generated with blastp using sets of representative
666 proteins selected after clustering using cd-hit with a 0.95 sequence identity cut-
667 off (Int, MpsA, TraG, SgaC) or a 0.90 sequence identity cut-off (TraN) [47].
668 Heatmaps showing the blastp identity scores were drawn using the Python library
669 seaborn v0.11.1 [48]. Circular blast representations (blast atlases) were
670 generated with the Blast Ring Image Generator (BRIG) 0.95 [49], with blastn or

671 blastp, against SGI1ΔIn104 and IE *VchUSA2*, with an upper identity threshold of
672 80% and a lower identity threshold of 60%. Antibiotic resistance gene prediction
673 was conducted using the Resistance Gene Identifier (RGI) software and CARD
674 3.1.3 database [50]. AcaCD binding motifs were identified using FIMO and MAST
675 [51] with the AcaCD motif matrix (S1 Matrix) described previously [17]. Logos for
676 *attL* and *attR* repeats were generated with MAST [51] using alignments of
677 sequences flanking the IE_{dusA} elements identified in this work.

678 **Phylogenetic analyses**

679 Evolutionary analyses were conducted in MEGA X [52] and inferred by using the
680 maximum likelihood method based on the JTT (MpsA or SgaC proteins), LG
681 (Int_{dusA}, Int_{yicC}, TraG or RepA_{IncFII} proteins) or WAG (TraN) matrix-based models
682 [53–55]. Protein sequences were aligned with Muscle [56]. Aligned sequences
683 were trimmed using trimal v1.2 using the automated heuristic approach [57].
684 Initial tree(s) for the heuristic search were obtained automatically by applying
685 Neighbor-Join and BioNJ algorithms to a matrix of pairwise distances estimated
686 using a JTT model, and then selecting the topology with the superior log
687 likelihood value. A discrete Gamma distribution was used to model evolutionary
688 rate differences among sites (5 categories) for Int_{dusA} (parameter = 3.5633), Int_{yicC}
689 (parameter = 2.6652), SgaC (parameter = 1.4064), TraG (parameter = 1.9005)
690 and TraN (parameter = 1.6476) proteins. For Int_{dusA}, MpsA and TraG, the rate
691 variation model allowed for some sites to be evolutionarily invariable ([+I], 7.81%
692 sites for Int_{dusA}, 44.62% sites for MpsA and 5.22% sites for TraG_S). The trees are
693 all drawn to scale, with branch lengths measured in the number of substitutions

694 per site. In all trees, bootstrap supports are shown as percentages at the
695 branching points only when > 80%.

696 *oriT* sequences were obtained manually using the previously identified *oriT* of
697 SGI1 as the reference [19], then clustered using cd-hit-est with a 1.0 nucleotide
698 sequence identity cut-off. Sequences were then aligned using Muscle and a
699 NeighborNet phylogenetic network was built using SplitsTree4 [58] with default
700 parameters (Uncorrected_P method for distances and EqualAngle drawing
701 method). The secondary structures of the aligned *oriT* sequences were predicted
702 using RNAalifold v2.4.17 from the ViennaRNA package [59]. Default options
703 were used (including no RIBOSUM scoring), except for the following: no
704 substituting "T" for "U" (--noconv), no lonely pairs (--noLP), no GU pairs (--noGU)
705 and DNA parameters (-P DNA). The predicted Vienna output and the annotated
706 alignment were merged into a predicted secondary structure of SGI1 *oriT* color-
707 coded to display the inter-island diversity.

708 **Statistical analyses and figures preparation**

709 Numerical data presented in graphs are available in S3 Dataset. Prism 8
710 (GraphPad Software) was used to plot graphics and to carry out statistical
711 analyses. All figures were prepared using Inkscape 1.0 (<https://inkscape.org/>).

712 **Acknowledgments**

713 We are grateful to Yann Boucher for the kind gift of *Vibrio cholerae* OYP6G08
714 and Kévin T. Huguet for technical assistance. We thank Nicolas Rivard and
715 David Roy for their insightful comments on the manuscript.

716 References

- 717 1. Bellanger X, Payot S, Leblond-Bourget N, Guédon G. Conjugative and
718 mobilizable genomic islands in bacteria: evolution and diversity. *FEMS*
719 *Microbiol Rev.* 2014;38: 720–760. doi:10.1111/1574-6976.12058
- 720 2. Guédon G, Libante V, Coluzzi C, Payot S, Leblond-Bourget N. The Obscure
721 World of Integrative and Mobilizable Elements, Highly Widespread Elements
722 that Pirate Bacterial Conjugative Systems. *Genes.* 2017;8: 337.
723 doi:10.3390/genes8110337
- 724 3. Daccord A, Ceccarelli D, Burrus V. Integrating conjugative elements of the
725 SXT/R391 family trigger the excision and drive the mobilization of a new
726 class of *Vibrio* genomic islands. *Mol Microbiol.* 2010;78: 576–588.
727 doi:10.1111/j.1365-2958.2010.07364.x
- 728 4. Daccord A, Ceccarelli D, Rodrigue S, Burrus V. Comparative analysis of
729 mobilizable genomic islands. *J Bacteriol.* 2013;195: 606–614.
730 doi:10.1128/JB.01985-12
- 731 5. Waldor MK. Mobilizable genomic islands: going mobile with *oriT* mimicry.
732 *Mol Microbiol.* 2010;78: 537–540. doi:10.1111/j.1365-2958.2010.07365.x
- 733 6. Carraro N, Rivard N, Ceccarelli D, Colwell RR, Burrus V. IncA/C Conjugative
734 Plasmids Mobilize a New Family of Multidrug Resistance Islands in Clinical
735 *Vibrio cholerae* Non-O1/Non-O139 Isolates from Haiti. *mBio.* 2016;7:
736 e00509-16. doi:10.1128/mBio.00509-16
- 737 7. de Curraize C, Siebor E, Neuwirth C. Genomic islands related to *Salmonella*
738 genomic island 1; integrative mobilisable elements in *trmE* mobilised in trans
739 by A/C plasmids. *Plasmid.* 2021;114: 102565.
740 doi:10.1016/j.plasmid.2021.102565
- 741 8. Mulvey MR, Boyd DA, Olson AB, Doublet B, Cloeckaert A. The genetics of
742 *Salmonella* genomic island 1. *Microbes and Infection.* 2006;8: 1915–1922.
743 doi:10.1016/j.micinf.2005.12.028
- 744 9. Boyd D, Peters GA, Cloeckaert A, Boumedine KS, Chaslus-Dancla E,
745 Imberechts H, et al. Complete nucleotide sequence of a 43-kilobase
746 genomic island associated with the multidrug resistance region of
747 *Salmonella enterica* serovar Typhimurium DT104 and its identification in
748 phage type DT120 and serovar Agona. *J Bacteriol.* 2001;183: 5725–5732.
749 doi:10.1128/JB.183.19.5725-5732.2001
- 750 10. Grim CJ, Hasan NA, Taviani E, Haley B, Chun J, Brettin TS, et al. Genome
751 sequence of hybrid *Vibrio cholerae* O1 MJ-1236, B-33, and CIRS101 and

- 752 comparative genomics with *V. cholerae*. J Bacteriol. 2010;192: 3524–3533.
753 doi:10.1128/JB.00040-10
- 754 11. Cummins ML, Hamidian M, Djordjevic SP. *Salmonella* Genomic Island 1 is
755 Broadly Disseminated within Gammaproteobacteriaceae. Microorganisms.
756 2020;8: 161. doi:10.3390/microorganisms8020161
- 757 12. Hall RM. *Salmonella* genomic islands and antibiotic resistance in *Salmonella*
758 *enterica*. Future Microbiol. 2010;5: 1525–1538. doi:10.2217/fmb.10.122
- 759 13. Doublet B, Boyd D, Mulvey MR, Cloeckert A. The *Salmonella* genomic
760 island 1 is an integrative mobilizable element. Mol Microbiol. 2005;55: 1911–
761 1924. doi:10.1111/j.1365-2958.2005.04520.x
- 762 14. Douard G, Praud K, Cloeckert A, Doublet B. The *Salmonella* genomic
763 island 1 is specifically mobilized in trans by the IncA/C multidrug resistance
764 plasmid family. PLoS ONE. 2010;5: e15302.
765 doi:10.1371/journal.pone.0015302
- 766 15. Harmer CJ, Hall RM. The A to Z of A/C plasmids. Plasmid. 2015;80: 63–82.
767 doi:10.1016/j.plasmid.2015.04.003
- 768 16. Wu W, Feng Y, Tang G, Qiao F, McNally A, Zong Z. NDM Metallo- β -
769 Lactamases and Their Bacterial Producers in Health Care Settings. Clin
770 Microbiol Rev. 2019;32: e00115-18. doi:10.1128/CMR.00115-18
- 771 17. Carraro N, Matteau D, Luo P, Rodrigue S, Burrus V. The master activator of
772 IncA/C conjugative plasmids stimulates genomic islands and multidrug
773 resistance dissemination. PLoS Genet. 2014;10: e1004714.
774 doi:10.1371/journal.pgen.1004714
- 775 18. Kiss J, Papp PP, Szabó M, Farkas T, Murányi G, Szakállas E, et al. The
776 master regulator of IncA/C plasmids is recognized by the *Salmonella*
777 Genomic island SGI1 as a signal for excision and conjugal transfer. Nucleic
778 Acids Res. 2015;43: 8735–8745. doi:10.1093/nar/gkv758
- 779 19. Kiss J, Szabó M, Hegyi A, Douard G, Praud K, Nagy I, et al. Identification
780 and Characterization of *oriT* and Two Mobilization Genes Required for
781 Conjugative Transfer of *Salmonella* Genomic Island 1. Front Microbiol.
782 2019;10: 457. doi:10.3389/fmicb.2019.00457
- 783 20. Huguet KT, Rivard N, Garneau D, Palanee J, Burrus V. Replication of the
784 *Salmonella* Genomic Island 1 (SGI1) triggered by helper IncC conjugative
785 plasmids promotes incompatibility and plasmid loss. PLoS Genet. 2020;16:
786 e1008965. doi:10.1371/journal.pgen.1008965

- 787 21. Szabó M, Murányi G, Kiss J. IncC helper dependent plasmid-like replication
788 of *Salmonella* Genomic Island 1. *Nucleic Acids Research*. 2021;49: 832–
789 846. doi:10.1093/nar/gkaa1257
- 790 22. Durand R, Huguet KT, Rivard N, Carraro N, Rodrigue S, Burrus V. Crucial
791 role of *Salmonella* genomic island 1 master activator in the parasitism of
792 IncC plasmids. *Nucleic Acids Res*. 2021; in press. doi:10.1093/nar/gkab204
- 793 23. Harmer CJ, Hamidian M, Ambrose SJ, Hall RM. Destabilization of IncA and
794 IncC plasmids by SGI1 and SGI2 type *Salmonella* genomic islands.
795 *Plasmid*. 2016;87–88: 51–57. doi:10.1016/j.plasmid.2016.09.003
- 796 24. Huguet KT, Gonnet M, Doublet B, Cloeckert A. A toxin antitoxin system
797 promotes the maintenance of the IncA/C-mobilizable *Salmonella* Genomic
798 Island 1. *Sci Rep*. 2016;6: 32285. doi:10.1038/srep32285
- 799 25. Carraro N, Durand R, Rivard N, Anquetil C, Barrette C, Humbert M, et al.
800 *Salmonella* genomic island 1 (SGI1) reshapes the mating apparatus of IncC
801 conjugative plasmids to promote self-propagation. *PLOS Genetics*. 2017;13:
802 e1006705. doi:10.1371/journal.pgen.1006705
- 803 26. Humbert M, Huguet KT, Coulombe F, Burrus V. Entry Exclusion of
804 Conjugative Plasmids of the IncA, IncC, and Related Untyped Incompatibility
805 Groups. *J Bacteriol*. 2019;201: e00731-18. doi:10.1128/JB.00731-18
- 806 27. Roberts AP, Johanesen PA, Lyras D, Mullany P, Rood JI. Comparison of
807 Tn5397 from *Clostridium difficile*, Tn916 from *Enterococcus faecalis* and the
808 CW459tet(M) element from *Clostridium perfringens* shows that they have
809 similar conjugation regions but different insertion and excision modules.
810 *Microbiology*. 2001;147: 1243–1251. doi:10.1099/00221287-147-5-1243
- 811 28. Burrus V, Pavlovic G, Decaris B, Guédon G. The ICES_{t1} element of
812 *Streptococcus thermophilus* belongs to a large family of integrative and
813 conjugative elements that exchange modules and change their specificity of
814 integration. *Plasmid*. 2002;48: 77–97. doi:10.1016/s0147-619x(02)00102-6
- 815 29. Bioteau A, Durand R, Burrus V. Redefinition and unification of the SXT/R391
816 Family of integrative and conjugative elements. *Appl Environ Microbiol*.
817 2018;84: pii: e00485-18. doi:10.1128/AEM.00485-18
- 818 30. Farrugia DN, Elbourne LDH, Mabbutt BC, Paulsen IT. A novel family of
819 integrases associated with prophages and genomic islands integrated within
820 the tRNA-dihydrouridine synthase A (*dusA*) gene. *Nucleic Acids Res*.
821 2015;43: 4547–4557. doi:10.1093/nar/gkv337
- 822 31. Daccord A, Mursell M, Poulin-Laprade D, Burrus V. Dynamics of the SetCD-
823 regulated integration and excision of genomic islands mobilized by

- 824 integrating conjugative elements of the SXT/R391 family. *J Bacteriol.*
825 2012;194: 5794–5802. doi:10.1128/JB.01093-12
- 826 32. Rivard N, Colwell RR, Burrus V. Antibiotic Resistance in *Vibrio cholerae*:
827 Mechanistic Insights from IncC Plasmid-Mediated Dissemination of a Novel
828 Family of Genomic Islands Inserted at *trmE*. *mSphere*. 2020;5: e00748-20.
829 doi:10.1128/mSphere.00748-20
- 830 33. Thorsted PB, Shah DS, Macartney D, Kostelidou K, Thomas CM.
831 Conservation of the genetic switch between replication and transfer genes of
832 IncP plasmids but divergence of the replication functions which are major
833 host-range determinants. *Plasmid*. 1996;36: 95–111.
834 doi:10.1006/plas.1996.0037
- 835 34. Roy D, Huguet KT, Grenier F, Burrus V. IncC conjugative plasmids and
836 SXT/R391 elements repair double-strand breaks caused by CRISPR-Cas
837 during conjugation. *Nucleic Acids Res.* 2020;48: 8815–8827.
838 doi:10.1093/nar/gkaa518
- 839 35. Carraro N, Sauvé M, Matteau D, Lauzon G, Rodrigue S, Burrus V.
840 Development of pVCR94ΔX from *Vibrio cholerae*, a prototype for studying
841 multidrug resistant IncA/C conjugative plasmids. *Front Microbiol.* 2014;5: 44.
842 doi:10.3389/fmicb.2014.00044
- 843 36. Doublet B, Golding GR, Mulvey MR, Cloeckaert A. Secondary Chromosomal
844 Attachment Site and Tandem Integration of the Mobilizable *Salmonella*
845 Genomic Island 1. Fairhead C, editor. *PLoS ONE*. 2008;3: e2060.
846 doi:10.1371/journal.pone.0002060
- 847 37. Hochhut B, Waldor MK. Site-specific integration of the conjugal *Vibrio*
848 *cholerae* SXT element into *prfC*. *Mol Microbiol.* 1999;32: 99–110.
- 849 38. de Curraize C, Siebor E, Neuwirth C, Hall RM. SGI0, a relative of
850 *Salmonella* genomic islands SGI1 and SGI2, lacking a class 1 integron,
851 found in *Proteus mirabilis*. *Plasmid*. 2019; 102453.
852 doi:10.1016/j.plasmid.2019.102453
- 853 39. Dower WJ, Miller JF, Ragsdale CW. High efficiency transformation of *E. coli*
854 by high voltage electroporation. *Nucleic Acids Res.* 1988;16: 6127–6145.
- 855 40. Demarre G, Guérout A-M, Matsumoto-Mashimo C, Rowe-Magnus DA,
856 Marlière P, Mazel D. A new family of mobilizable suicide plasmids based on
857 broad host range R388 plasmid (IncW) and RP4 plasmid (IncPalpha)
858 conjugative machineries and their cognate *Escherichia coli* host strains. *Res*
859 *Microbiol.* 2005;156: 245–255. doi:10.1016/j.resmic.2004.09.007

- 860 41. Datsenko KA, Wanner BL. One-step inactivation of chromosomal genes in
861 *Escherichia coli* K-12 using PCR products. Proc Natl Acad Sci U S A.
862 2000;97: 6640–6645.
- 863 42. Datta S, Costantino N, Court DL. A set of recombineering plasmids for
864 gram-negative bacteria. Gene. 2006;379: 109–115.
865 doi:10.1016/j.gene.2006.04.018
- 866 43. Cherepanov PP, Wackernagel W. Gene disruption in *Escherichia coli*: TcR
867 and KmR cassettes with the option of Flp-catalyzed excision of the
868 antibiotic-resistance determinant. Gene. 1995;158: 9–14. doi:10.1016/0378-
869 1119(95)00193-a
- 870 44. Haldimann A, Wanner BL. Conditional-replication, integration, excision, and
871 retrieval plasmid-host systems for gene structure-function studies of
872 bacteria. J Bacteriol. 2001;183: 6384–6393. doi:10.1128/JB.183.21.6384-
873 6393.2001
- 874 45. Senanayake SD, Brian DA. Precise large deletions by the PCR-based
875 overlap extension method. Mol Biotechnol. 1995;4: 13.
876 doi:10.1007/BF02907467
- 877 46. Hellemans J, Mortier G, De Paepe A, Speleman F, Vandesompele J. qBase
878 relative quantification framework and software for management and
879 automated analysis of real-time quantitative PCR data. Genome Biology.
880 2007;8: R19. doi:10.1186/gb-2007-8-2-r19
- 881 47. Li W, Godzik A. Cd-hit: a fast program for clustering and comparing large
882 sets of protein or nucleotide sequences. Bioinformatics. 2006;22: 1658–
883 1659. doi:10.1093/bioinformatics/btl158
- 884 48. Waskom M. seaborn: statistical data visualization. JOSS. 2021;6: 3021.
885 doi:10.21105/joss.03021
- 886 49. Alikhan N-F, Petty NK, Ben Zakour NL, Beatson SA. BLAST Ring Image
887 Generator (BRIG): simple prokaryote genome comparisons. BMC
888 Genomics. 2011;12: 402. doi:10.1186/1471-2164-12-402
- 889 50. Alcock BP, Raphenya AR, Lau TTY, Tsang KK, Bouchard M, Edalatmand A,
890 et al. CARD 2020: antibiotic resistome surveillance with the comprehensive
891 antibiotic resistance database. Nucleic Acids Res. 2020;48: D517–D525.
892 doi:10.1093/nar/gkz935
- 893 51. Bailey TL, Boden M, Buske FA, Frith M, Grant CE, Clementi L, et al. MEME
894 SUITE: tools for motif discovery and searching. Nucleic Acids Res. 2009;37:
895 W202-208. doi:10.1093/nar/gkp335

- 896 52. Kumar S, Stecher G, Li M, Knyaz C, Tamura K. MEGA X: Molecular
897 Evolutionary Genetics Analysis across Computing Platforms. *Mol Biol Evol.*
898 2018;35: 1547–1549. doi:10.1093/molbev/msy096
- 899 53. Jones DT, Taylor WR, Thornton JM. The rapid generation of mutation data
900 matrices from protein sequences. *Bioinformatics.* 1992;8: 275–282.
901 doi:10.1093/bioinformatics/8.3.275
- 902 54. Whelan S, Goldman N. A General Empirical Model of Protein Evolution
903 Derived from Multiple Protein Families Using a Maximum-Likelihood
904 Approach. *Mol Biol Evol.* 2001;18: 691–699.
905 doi:10.1093/oxfordjournals.molbev.a003851
- 906 55. Le SQ, Gascuel O. An Improved General Amino Acid Replacement Matrix.
907 *Mol Biol Evol.* 2008;25: 1307–1320. doi:10.1093/molbev/msn067
- 908 56. Edgar RC. MUSCLE: multiple sequence alignment with high accuracy and
909 high throughput. *Nucleic Acids Res.* 2004;32: 1792–1797.
910 doi:10.1093/nar/gkh340
- 911 57. Capella-Gutiérrez S, Silla-Martínez JM, Gabaldón T. trimAl: a tool for
912 automated alignment trimming in large-scale phylogenetic analyses.
913 *Bioinformatics.* 2009;25: 1972–1973. doi:10.1093/bioinformatics/btp348
- 914 58. Huson DH, Bryant D. Application of Phylogenetic Networks in Evolutionary
915 Studies. *Molecular Biology and Evolution.* 2006;23: 254–267.
916 doi:10.1093/molbev/msj030
- 917 59. Lorenz R, Bernhart SH, Höner zu Siederdissen C, Tafer H, Flamm C,
918 Stadler PF, et al. ViennaRNA Package 2.0. *Algorithms Mol Biol.* 2011;6: 26.
919 doi:10.1186/1748-7188-6-26
- 920 60. Kirchberger PC, Orata FD, Nasreen T, Kauffman KM, Tarr CL, Case RJ, et
921 al. Culture-independent tracking of *Vibrio cholerae* lineages reveals complex
922 spatiotemporal dynamics in a natural population. *Environ Microbiol.* 2020;22:
923 4244–4256. doi:10.1111/1462-2920.14921
- 924 61. Heidelberg JF, Eisen JA, Nelson WC, Clayton RA, Gwinn ML, Dodson RJ,
925 et al. DNA sequence of both chromosomes of the cholera pathogen *Vibrio*
926 *cholerae*. *Nature.* 2000;406: 477–483. doi:10.1038/35020000
- 927 62. Singer M, Baker TA, Schnitzler G, Deischel SM, Goel M, Dove W, et al. A
928 collection of strains containing genetically linked alternating antibiotic
929 resistance elements for genetic mapping of *Escherichia coli*. *Microbiol Rev.*
930 1989;53: 1–24.
- 931 63. Ceccarelli D, Daccord A, René M, Burrus V. Identification of the Origin of
932 Transfer (*oriT*) and a New Gene Required for Mobilization of the SXT/R391

- 933 Family of Integrating Conjugative Elements. *J Bacteriol.* 2008;190: 5328–
934 5338. doi:10.1128/JB.00150-08
- 935 64. Grenier F, Matteau D, Baby V, Rodrigue S. Complete genome sequence of
936 *Escherichia coli* BW25113. *Genome Announc.* 2014;2: pii: e01038-14.
937 doi:10.1128/genomeA.01038-14
- 938 65. Garriss G, Waldor MK, Burrus V. Mobile antibiotic resistance encoding
939 elements promote their own diversity. *PLoS Genet.* 2009;5: e1000775.
940 doi:10.1371/journal.pgen.1000775
- 941 66. Guzman LM, Belin D, Carson MJ, Beckwith J. Tight regulation, modulation,
942 and high-level expression by vectors containing the arabinose P_{BAD}
943 promoter. *J Bacteriol.* 1995;177: 4121–4130.
- 944

945 **Table 1. Main features of the IEs described in this study.**

IE Name	Organism ¹	Size (bp)	Target site	Genbank accession number
GI VchRus1	<i>V. cholerae</i> 1	30,204	<i>dusA</i>	NZ_SMZE01000022
IE VchAus1	<i>V. cholerae</i> A12JL36W30	27,410	<i>dusA</i>	NZ_VIOZ01000074
IE VchUSA5	<i>V. cholerae</i> OYP2C05	28,706	<i>dusA</i>	NZ_NMTM01000021
IME VchUSA3	<i>V. cholerae</i> OYP6G08	30,910	<i>dusA</i>	NZ_NMSY01000009
IE VchA215 ²	<i>V. cholerae</i> A215 sv Inaba	29,933	<i>dusA</i>	CWPR01000020.1
IE VchUSA2	<i>V. cholerae</i> 692-79	29,931	<i>dusA</i>	MIPA01000024
IE VchN2751 ²	<i>V. cholerae</i> N2751	30,018	<i>dusA</i>	NZ_VSGL01000012
IE VchN2744 ²	<i>V. cholerae</i> N2744	30,134	<i>dusA</i>	NZ_VSGF01000021.1
IE VchN2708	<i>V. cholerae</i> N2708	27,248	<i>dusA</i>	NZ_VSFQ01000013
IE VchN2786	<i>V. cholerae</i> N2786	24,658	<i>dusA</i>	NZ_VSHP01000008
IE VchN2817	<i>V. cholerae</i> N2817	28,717	<i>dusA</i>	NZ_VSIM01000004
IE VchChn1	<i>V. cholerae</i> N2787	27,195	<i>dusA</i>	NZ_VSHQ01000015
IE VchBan1	<i>V. cholerae</i> EM-1676-A	36,519	<i>dusA</i>	NZ_KB662834
IE VchHai10	<i>V. cholerae</i> 2012Env-2	37,162	<i>dusA</i>	NZ_JSTD01000059/60
IE VchSwe1	<i>V. cholerae</i> 11116	28,100	<i>dusA</i>	NZ_MDYK01000006
IE VchBra2	<i>V. cholerae</i> TMA-21	28,230	<i>dusA</i>	ACHY01000008
IE VmeUSA1	<i>V. metoecus</i> 07-2435	23,518	<i>dusA</i>	NZ_LCUE01000016
IE VpaChn1	<i>V. parahaemolyticus</i> GIMxtf41-2013.07	28,589	<i>dusA</i>	NZ_MRWJ01000014
IE VpaChn2	<i>V. parahaemolyticus</i> C2_8	25,944	<i>dusA</i>	NZ_NNLT01000047
IE VpaBan1a	<i>V. parahaemolyticus</i> NIHCB0757	29,418	<i>dusA</i>	AVPX01000004
IE VvuUSA1	<i>V. vulnificus</i> VA-WGS-18041	30,228	<i>dusA</i>	NZ_RBZL01000019
IE EcoMOD1	<i>E. coli</i> MOD1-EC5437	25,611	<i>yicC</i>	NZ_NLPO01000006
IE SenUSA1	<i>S. enterica</i> Kentucky ARS-CC8289	25,970	<i>yicC</i>	NZ_MCPS01000044
IE PplInd1	<i>P. plantistimulans</i> L1E11	22,777	<i>yicC</i>	NZ_LAPT01000132/095
GI VchO27-1	<i>V. cholerae</i> 10432-62	26,646	<i>trmE</i>	CP010812

946 ¹ *V.*, *Vibrio*; *E.*, *Escherichia*; *S.*, *Salmonella*; *P.*, *Pokkaliibacter*

947 ² Not represented in Fig 1 as nucleotide sequences contain gaps

948 **Table 2. Strains and elements used in this study.**

Strains or elements	Relevant genotype or phenotype ^a	Source or reference
<i>V. cholerae</i>		
OY6PG08	Environmental, Oyster Pond, MA, USA, August 2009	[60]
N16961	O1 El Tor	[61]
<i>E. coli</i>		
β2163	(F ⁻) RP4-2-Tc::Mu Δ <i>dapA</i> ::(<i>erm-pir</i>) (Kn Em)	[40]
CAG18439	MG1655 <i>lacZU118 lacI42</i> ::Tn10 (Tc)	[62]
BW25113	F ⁻ Δ(<i>araD-araB</i>)567, Δ <i>lacZ4787</i> ::(<i>rrnB-3</i>), λ ⁻ , <i>rph-1</i> , Δ(<i>rhaD-rhaB</i>)568, <i>hsdR514</i>	[41]
EC100	F <i>mcrA</i> Δ(<i>mrr-hsdRMS-mcrBC</i>) Φ80 <i>dlacZΔM15 ΔlacX74 recA1 endA1 araD139 Δ(ara, leu)7697 galU galK λ⁻ rpsL (Sm^R) nupG</i>	Epicentre, Madison Wis.
KH40	MG1655 Δ <i>dapA</i> :: <i>cat</i> (Cm)	This study
VB112	Rf-derivative of MG1655	[63]
GG56	Nx-derivative of BW25113	[35,64]
FD034	CAG18439 Δ <i>lacZ dusA'</i> -' <i>lacZ-aad7</i> (Tc Sp)	This study
FD036	GG56 <i>dusA'</i> -' <i>lacZ-aad7</i> (Nx Sp)	This study
Plasmids		
pKD3	Cm ^R PCR template for one-step chromosomal gene inactivation (Cm)	[41]
pKD4	Kn ^R PCR template for one-step chromosomal gene inactivation (Kn)	[41]
pKD13	Kn ^R PCR template for one-step chromosomal gene inactivation (Kn)	[41]
pVI36	Sp ^R PCR template for one-step chromosomal gene inactivation (Sp)	[63]
pVI42B	pVI36 BamHI::P _{lac} - <i>lacZ</i> (Sp)	[65]
pSW23T	pSW23:: <i>oriT</i> _{RP4} ; <i>oriV</i> _{R6KY} (Cm)	[40]
pOP <i>lacZ</i>	pAH56 <i>lacZ</i> (Kn)	[17]
pBAD30	<i>ori</i> _{p15A} <i>bla araC P</i> _{BAD} (Ap)	[66]
pBAD- <i>acaDC</i>	pBAD30:: <i>acaDC</i> (Ap)	[17]
pBAD- <i>rdfN</i>	pBAD30:: <i>rdfN</i> (Ap)	This study
pBAD- <i>sgaC</i>	pBAD30:: <i>sgaC</i> (Ap)	This study
pVCR94 ^{Kn} Δ <i>acr2</i>	Δ <i>acr2</i> mutant of pVCR94 ^{Kn} (Su Kn)	[34]
pVCR94 ^{Sp}	Sp ^R derivative of pVCR94 (Su Sp)	[17]
pVCR94 ^{Sp} Δ <i>acaC</i>	Δ <i>acaC</i> mutant of pVCR94 ^{Sp} (Su Sp)	[17]
pVCR94 ^{Sp} Δ <i>acaDC</i>	Δ <i>acaDC</i> mutant of pVCR94 ^{Sp} (Su Sp)	[17]
Integrative elements		
IME <i>VchUSA3</i>		This study
IME <i>VchUSA3</i> ^{Cm}	IME <i>VchUSA3</i> CGT85_RS05425ΩpSW23T (Cm)	This study
IME <i>VchUSA3</i> ^{Kn}	Kn ^R derivative of IME <i>VchUSA3</i> (Kn)	This study
IME <i>VchUSA3</i> ^{Kn} Δ <i>sgaC</i>	Δ <i>sgaC</i> mutant of IME <i>VchUSA3</i> (Kn)	This study
IME <i>VchUSA3</i> ^{Kn} Δ <i>rdfN</i>	Δ <i>rdfN</i> mutant of IME <i>VchUSA3</i> (Kn)	This study
mini-IE	<i>attP-int-aad7</i> derived from IME <i>VchUSA3</i> (Sp)	This study

949 ^aAp, ampicillin; Cm, chloramphenicol; Em, erythromycin, Kn, kanamycin; Nx, Nalidixic

950 acid; Rf, rifampin; Sm, streptomycin; Sp, spectinomycin; Su, sulfamethoxazole; Tc,

951 tetracycline; Tm, trimethoprim; ts, thermosensitive.

952 **Supporting information**

953 **S1 Fig. Comparative sequence analysis of SGI1-like *dusA*-specific IEs.** Blastn and
954 blastp atlases using either SGI1ΔIn104 (A) or IE *VchUSA2* (B) as the reference. Coding
955 sequences appear on the outermost circle in blue for the positive strand and red for the
956 negative strand, with the *oriT* depicted as a grey arc. All other sequences are
957 represented only according to their homology with the reference, with full opacity
958 corresponding to 100% identity and gaps indicating identity below 60%. The order of the
959 IEs in the atlases is indicated according to the color keys shown in the inset of panel B.

960 **S2 Fig. NeighborNet phylogenetic network and predicted secondary structure of**
961 **39 *oriT* loci of SGI1-like IEs.** Each IE's integration site and type are annotated. The
962 sequence of canonical SGI1 (Genbank AF261825.2) was used as a reference to show
963 the predicted secondary structure of all *oriT* sequences. Pairs can be perfectly
964 conserved, imperfectly conserved (1/39 not conserved), not conserved (> 1/39), or an A-
965 T or G-C pair only. In the latter case, the sequence is not conserved, but the predicted
966 local secondary structure is.

967 **S3 Figure. Maximum likelihood phylogenetic analysis of key proteins of SGI1-**
968 **related IEs.** The trees for MpsA (A), TraG (B), SgaC (C) and TraN (D) proteins are
969 drawn to scale, with branch lengths measured in the number of substitutions per site
970 over 321, 1,145, 188, and 968 amino acid positions, respectively. For clarity, the lengths
971 of the branches linking the two groups in panels A and C were artificially divided by 8
972 and 4, respectively. Taxa corresponding to IEs targeting *trmE* and *yicC* are shown by a
973 light blue circle and a red circle, respectively. All other taxa correspond to *dusA*-specific
974 IEs. Proteins accession numbers are provided in S1 Table and S2 Dataset.

975 **S4 Figure. Alignment of AcaCD-responsive promoters predicted in IEs targeting**
976 ***dusA*, *yicC* and *trmE*.** Promoter sequences are grouped based on the function of the
977 expressed genes as follows: (A) RDFs; (B) mating pair stabilization; (C) mating pair
978 formation and stabilization; (D) unknown. AcaCD binding sites are shown in green. Logo
979 sequences and *p*-values were generated by MAST [51]. Known transcription start sites
980 are shown in blue [17,22]. Predicted Shine-Dalgarno sequences are shown in pink. The
981 initiation start codon is shown in bold letters.

982 **S5 Figure. Excision of IME *VchUSA3* is enhanced in *IncC*⁺ cells.** (A) Model of
983 excision of IME *VchUSA3*. (B and C) Detection of *attB*, *attP*, *attL* and *attR* sites by PCR
984 in colonies of *V. cholerae* OYO6G08 bearing (lanes 9 to 16) or lacking (lanes 1 to 8)
985 pVCR94^{Kn} Δ *acr2*. Control lanes: L, 1Kb Plus DNA ladder (Transgen Biotech); +,
986 *V. cholerae* N16961 genomic DNA. (D) Detection of *attB*, *attP*, *attL* and *attR* sites by
987 PCR in transconjugant colonies of *E. coli* CAG18439 (lanes 1 to 4). L, 100bp Plus II
988 DNA Ladder (Transgen Biotech)

989 **S1 Table. Features of the identified IEs and associated strains.**

990 **S2 Table. Oligonucleotides used in this study.**

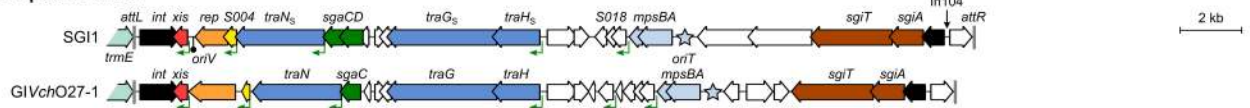
991 **S1 Dataset. Features of ORFs in the identified IEs.**

992 **S2 Dataset. Clusters generated by cd-hit for Int, MpsA, TraG, SgaC and TraN.**

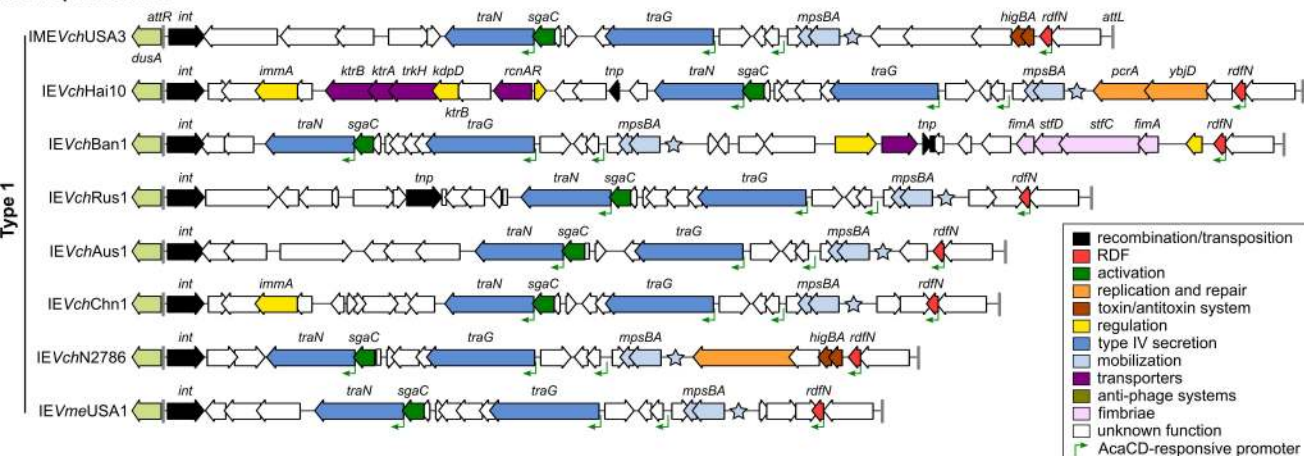
993 **S3 Dataset. Numerical data presented in Figs 4, 5 and 6.**

994 **S1 Matrix. AcaCD motif matrix to identify AcaCD binding sites.**

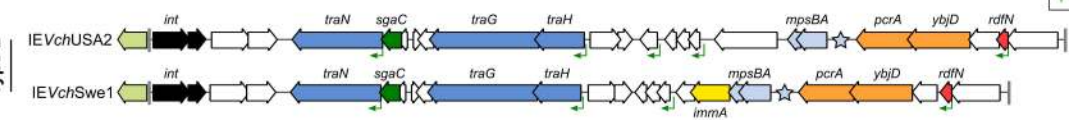
trmE-specific IMEs



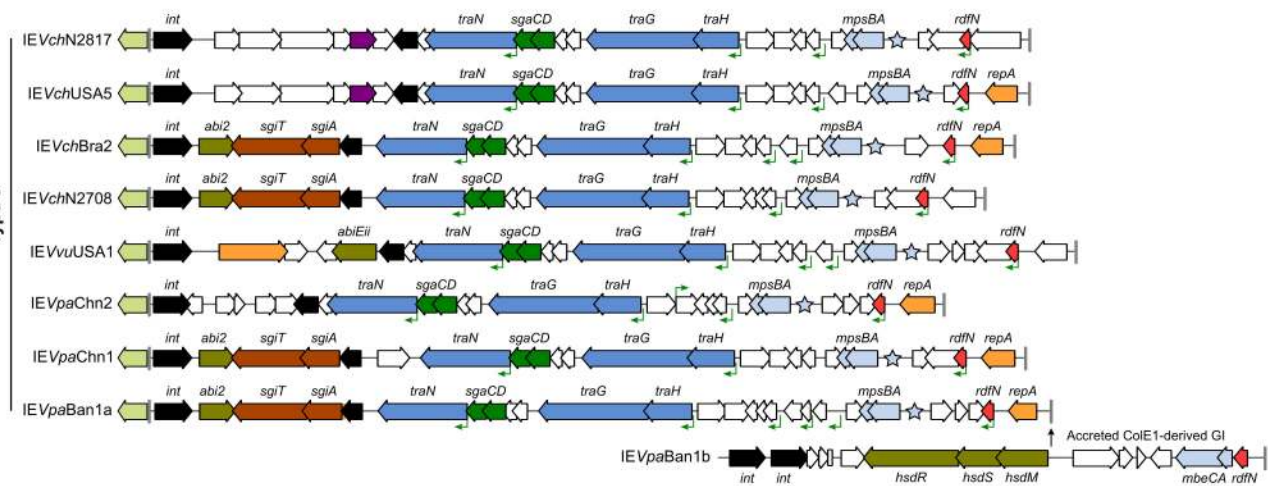
dusA-specific IMEs



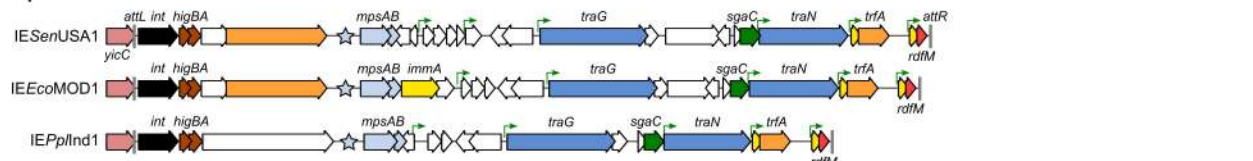
Type 2

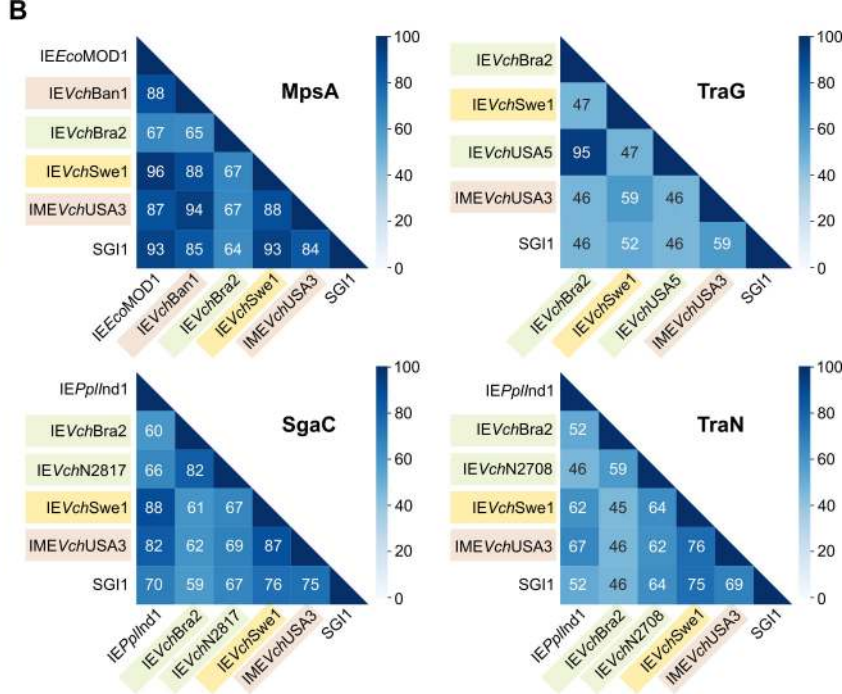
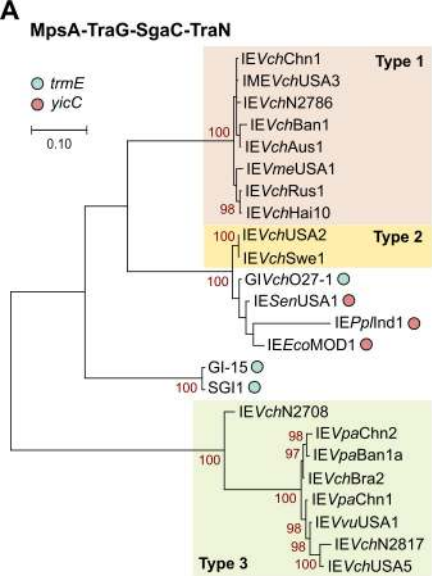


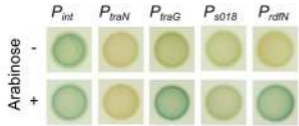
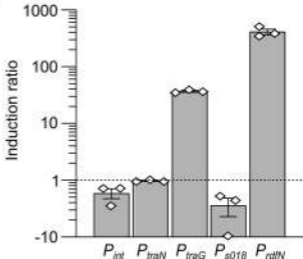
Type 3

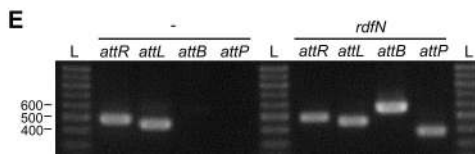
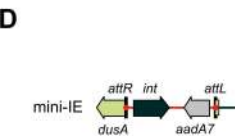
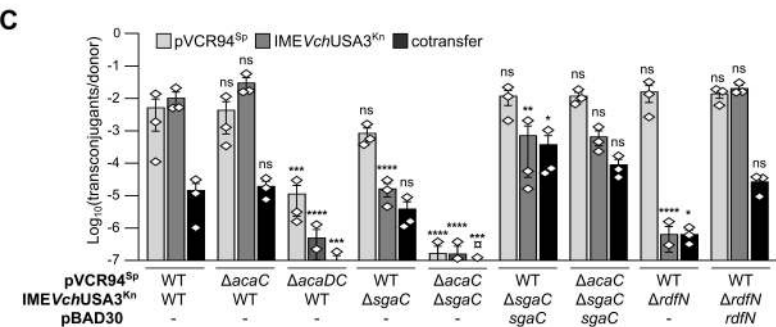
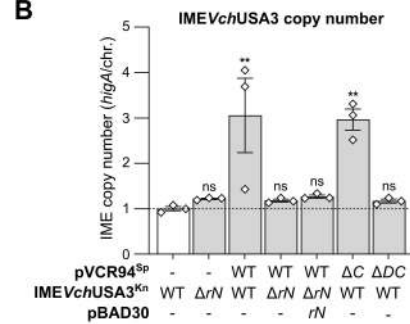
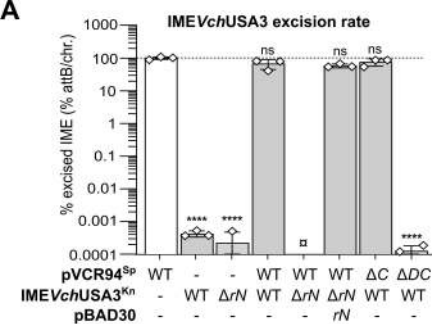


yicC-specific IMEs





A**B**

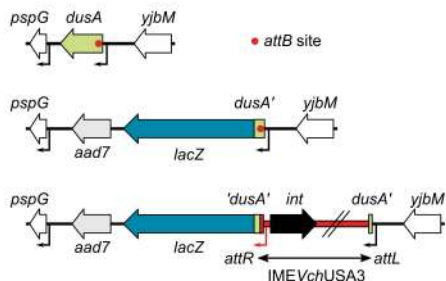


A*E. coli* K12 *dusA attB* site

TAATCTCTACATTTGAAA **ATG** CAC GGT AAT TCT GAA ATG CAA AAA ATC AAC CAA ACC AGC GCA ATG CCT GAA
M H G N S E M Q K I N Q T S A M P E
AAA ACT GAC GTT CAC TGG AGT GGT CGG TTT AGC **GTT GCA CCA ATG CTC GAC TGG** ACG GAC AGA CAT
K T D V H W S G R F S V A P M L D W T D R H

E. coli K12 *dusA::IMEVchUSA3^{Kn} attR* junction

AGTTGAGATTAGTTAAGA **ATG** AGC CAG AAA CAG AAT ACA GAT AAA TCT TTG CAA GAC AGT GAG TTA TCT AGT
M S Q K Q N T D K S L Q D S E L S S
AAT ATT GAT GTG TCA TTA AGT CGT AGA TTC AGC **GTG GCC CCC ATG CTT GAC TGG** ACG GAC AGA CAT
N I D V S L S R R F S V A P M L D W T D R H

B**C**